Polarimetric Decomposition Applied to 3D SAR Images of Forested Terrain.

Stefan Sauer, Florian Kugler, Seung-Kuk Lee, Kostas Papathanassiou
German Aerospace Center (DLR), Microwaves and Radar Institute (HR), Germany

Abstract

In this paper, recently conceived polarimetric array signal processing techniques are applied for producing 3D images over forested scenes from multibaseline POL-InSAR observations. Subsequently, the optimal scattering mechanisms are investigated using polarimetric decomposition to derive structural forest parameters. This three-dimensional analysis is performed by employing multibaseline POL-InSAR datasets over a temperate forest (Traunstein) acquired by the E-SAR system of DLR at L-band and validated against LIDAR measurements.

1 Introduction

While SAR polarimetry (POLSAR) permits the identification of elementary scattering processes inside the resolution cell, SAR interferometry (InSAR) determines the height of scatterers. Polarimetric SAR interferometry (POL-InSAR) allows the estimation of the vertical location of scattering mechanisms [1]. To extract physical parameters from single-baseline POL-InSAR observations different coherent models describing the reflection processes have been proposed [2]. Schemes to inverse the electromagnetic models for retrieving forest parameters such as tree height and underlying ground topography have been introduced [2, 3]. A three-dimensional model-based radar imaging technique of vegetation using single- and dual-baseline polarimetric interferometric SAR observations called Polarization Coherence Tomography has been developed lately [4].

An extension of conventional two-dimensional SAR imaging is SAR Tomography that permits the reconstruction of the three-dimensional scatterer distribution [5]. The tomographic imaging approach has been applied to forested areas where both the ground and the canopy have been distinguished resulting in an estimation of tree height and ground topography.

Recently, a new way of analyzing polarimetric multibaseline (MB) InSAR data has been conceived by adapting array signal processing algorithms to this configuration [6, 7]. These polarimetric methods permit the estimation of the reflector height, the scattering mechanism, and the polarimetric reflectivity. In this paper, they are applied for generating three-dimensional images of forested scenes from polarimetric multibaseline InSAR data. Subsequently, the with respect to the particular algorithm optimal scattering vectors are examined by a polarimetric decomposition approach [8]. The polarimetric multibaseline interferometric data at L-band were acquired by the E-SAR system of DLR over the temperate forest of Traunstein. The results are validated using LIDAR measurements [9, 10].

2 Polarimetric MB InSAR Array Signal Processing Techniques

In this section, spectral analysis techniques are extended to the fully polarimetric MB InSAR configuration. The following adaptation to the fully polarimetric case not merely increases the number of observables, but especially finds the optimal polarization combination for height estimation. Furthermore, these algorithms allow examining the scatterer physical properties by analysis of their polarimetric behavior.

2.1 Polarimetric MB InSAR Signal Model

The polarimetric multibaseline interferometric SAR received signal for p sensors is modeled as [7]

$$\mathbf{y}(n) \quad = \quad \sum_{i=1}^{N_s} \sqrt{\tau_i}\mathbf{x}_i(n) \odot \mathbf{b}(z_i, \mathbf{k}_i) + \mathbf{v}(n) \qquad (1)$$

with $n = 1, \ldots, N$, the number of looks N, and the Schur-Hadamard product $\odot$ (elementwise multiplication). The number of backscattering sources N_s is considered to be a deterministic parameter. The observation vector $\mathbf{y}(n) \in \mathbb{C}^{\tilde{p}}$, $\tilde{p} = 4p$, is a Gaussian random process with zero mean and covariance matrix $\mathbf{R}$. The polarimetric reflectivity τ and the height z of the scatterers are assumed to be deterministic unknown quantities. The additive white Gaussian noise is denoted by $\mathbf{v}(n)$, and the multiplicative noise by $\mathbf{x}_i(n)$.

The main modification with respect to the single polarization model [11] is the structure of the MB polarimetric interferometric (MBPI) steering vector $\mathbf{b}(z, \mathbf{k}) \in \mathbb{C}^{\tilde{p}}$. It is a linear combination of four steering vectors $\mathbf{a}_{\gamma_i}(z)$, each of them associated with one particular polarization [6, 7]

$$\mathbf{b}(z, \mathbf{k}) = k_1\mathbf{a}_{\gamma_1}(z) + k_2\mathbf{a}_{\gamma_2}(z) + k_3\mathbf{a}_{\gamma_3}(z) + k_4\mathbf{a}_{\gamma_4}(z) \qquad (2)$$

where

$$\mathbf{a}_{\gamma_i}(z) = \begin{bmatrix} \mathbf{0}_{(i-1)p\times 1} \\ \mathbf{a}(z) \\ \mathbf{0}_{(4-i)p\times 1} \end{bmatrix}. \quad (3)$$

The single polarization steering vector $\mathbf{a}(z) \in \mathbb{C}^p$ for a general acquisition geometry is represented as

$$\mathbf{a}(z) = [1, \exp(j\kappa_{z_2} z), \ldots, \exp(j\kappa_{z_p} z)]^T \quad (4)$$

with the vertical wavenumber $\kappa_{z_\nu} = \frac{4\pi}{\lambda}\frac{\Delta\theta_\nu}{\sin\theta_\nu}$. The complex weighting coefficients form a vector

$$\mathbf{k} = [k_1, k_2, k_3, k_4]^T \quad (5)$$

that is a scattering mechanism. This can be written in matrix notation as

$$\mathbf{b}(z, \mathbf{k}) = \mathbf{B}(z)\mathbf{k} \quad (6)$$

with the matrix of MBPI steering vectors

$$\mathbf{B}(z) = \left[\mathbf{a}_{\gamma_1}(z), \mathbf{a}_{\gamma_2}(z), \mathbf{a}_{\gamma_3}(z), \mathbf{a}_{\gamma_4}(z)\right]. \quad (7)$$

The estimate of the sample covariance matrix $\hat{\mathbf{R}} \in \mathbf{Mat}_{\tilde{p}}(\mathbb{C})$ is given by

$$\hat{\mathbf{R}} = \frac{1}{N}\sum_{n=1}^{N} \mathbf{y}(n)\mathbf{y}^H(n). \quad (8)$$

2.2 Polarimetric Beamforming

The spectrum of the polarimetric beamforming method is given by [7]

$$\hat{P}_{BF}^P(z) = \frac{\lambda_{\max}(\mathbf{B}^H(z)\hat{\mathbf{R}}\mathbf{B}(z))}{p^2}. \quad (9)$$

This means that for each frequency z the maximal eigenvalue and its corresponding eigenvector of the linear system

$$\mathbf{B}^H(z)\hat{\mathbf{R}}\mathbf{B}(z)\mathbf{k}_{\max} = \lambda_{\max}\mathbf{k}_{\max} \quad (10)$$

has to be computed. The eigenvector $\mathbf{k}_{\max}$ is a polarimetric scattering mechanism allowing a polarimetric analysis to retrieve the physical properties of the reflector. The frequency estimates $\hat{\boldsymbol{z}} = [\hat{z}_1, \ldots, \hat{z}_{N_s}]^T$ are related to the positions of the N_s largest peaks of the spectrum. The polarimetric reflectivity at frequency $\hat{z}_i$ is estimated by $\hat{\tau}_i = \hat{P}_{BF}^P(\hat{z}_i)$.

2.3 Polarimetric Capon Method

The spectrum of the polarimetric Capon algorithm is obtained as [7]

$$\hat{P}_{C}^P(z) = \frac{1}{\lambda_{\min}(\mathbf{B}^H(z)\hat{\mathbf{R}}^{-1}\mathbf{B}(z))}. \quad (11)$$

For each frequency z the minimal eigenvalue and associated eigenvector of the linear system

$$\mathbf{B}^H(z)\hat{\mathbf{R}}^{-1}\mathbf{B}(z)\mathbf{k}_{\min} = \lambda_{\min}\mathbf{k}_{\min} \quad (12)$$

has to be calculated. The polarimetric scattering type $\mathbf{k}_{\min}$ permits to extract the physical behavior of the scatterer. The frequency estimates $\hat{\boldsymbol{z}} = [\hat{z}_1, \ldots, \hat{z}_{N_s}]^T$ are given by the locations of the N_s maxima of the spectrum $\hat{P}_C^P$. The polarimetric reflectivity at frequency $\hat{z}_i$ is determined by $\hat{\tau}_i = \hat{P}_C^P(\hat{z}_i)$.

2.4 Polarimetric MUSIC Algorithm

If N_s is the assumed number of scatterers, the matrix of the noise eigenvectors is $\mathbf{E}_q \in \mathbb{C}^{\tilde{p}\times q}$ with $q = \tilde{p} - N_s$. The pseudo-spectrum of MUSIC for the fully polarimetric SAR configuration is [7]

$$\hat{P}_{MU}^P(z) = \frac{1}{\lambda_{\min}(\mathbf{B}^H(z)\mathbf{E}_q\mathbf{E}_q^H\mathbf{B}(z))} \quad (13)$$

with $\lambda_{\min}$ the smallest eigenvalue of the 4×4 Hermitian linear system

$$\mathbf{B}^H\mathbf{E}_q\mathbf{E}_q^H\mathbf{B}\mathbf{k}_{\min} = \lambda_{\min}\mathbf{k}_{\min}. \quad (14)$$

The eigenvector $\mathbf{k}_{\min}$ describes the physical features of the scatterer and permits a polarimetric analysis. The linear system (14) must be of full rank, otherwise $\lambda_{\min} = 0$. This leads to an infinite spectrum (13) and the height cannot be determined. A necessary criterion for the linear system having full rank is $\tilde{p} \geq N_s + 4$.

3 Experimental Results

The performance of the introduced algorithms is validated using fully polarimetric multibaseline interferometric datasets over a temperate forest (Traunstein). The measurements were acquired by the E-SAR system of DLR at L-band and consist of five tracks with nominal spatial baselines of 5 m. Furthermore, LIDAR data [9, 10] comprising topography height and h_{100} forest height is available for validation purposes.

3.1 3D Images

Figure 1 shows in 3D the optimal reflection vectors evaluated by beamforming, Capon, and MUSIC of model order four along a line of 121 samples. Since the spectral peaks of beamforming are quite large, this method is not appropriate for efficient focusing in the vertical direction. The polarimetric Capon algorithm and even to a greater extent the polarimetric MUSIC enhance the resolution and considerably suppress the sidelobes. These methods are capable to extract several components within one azimuth-range resolution cell: one at the ground, others inside the forest volume beneath the forest height measured by the LIDAR system. This behavior can be explained by the property of electromagnetic waves at L-band to penetrate into a semi-transparent volume. The defocusing on the right hand side for the MUSIC approach is due to overmodeling and does not occur for model orders one and two.

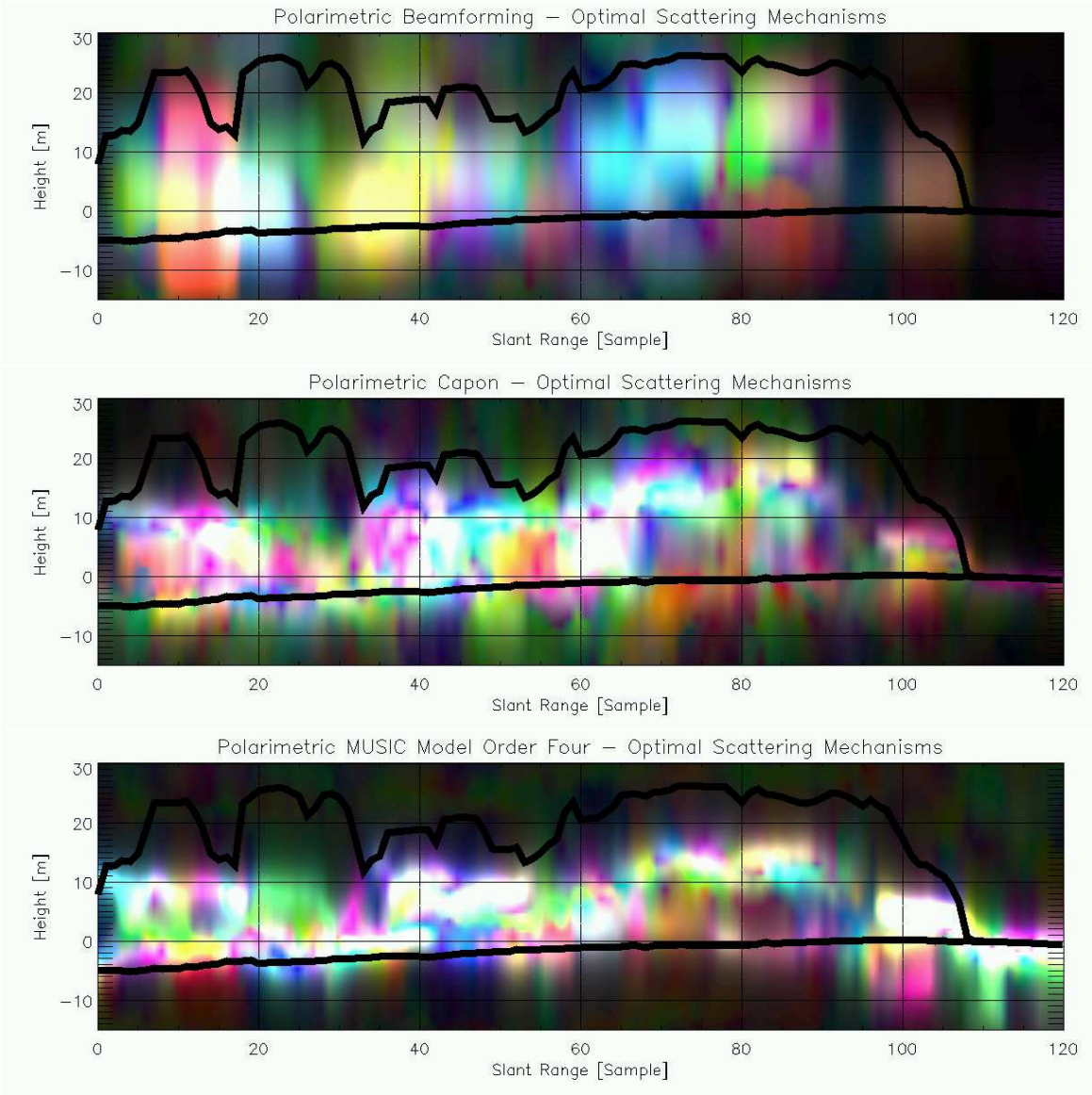

Figure 1: 3D optimal scattering mechanisms in the Pauli polarization basis. Top: Polarimetric beamforming, middle: Polarimetric Capon, bottom: Polarimetric MUSIC with model order four.

Figure 2: Three-component decomposition of polarimetric MUSIC with model order four: Double-bounce red, surface reflection blue, volume diffusion green.

3.2 Polarimetric Decomposition

To investigate in further detail the reflection processes occurring inside a forest already visible in the 3D images of the optimal scattering mechanisms, they are analyzed by the polarimetric three-component decomposition. This polarimetric decomposition is based on the model introduced in [8] that includes three scattering mechanisms, namely canopy (or volume), double-bounce, and surface scattering. The model for the total backscatter is given by [8]

$$\begin{aligned} \langle S_{hh}S_{hh}^* \rangle &= f_s|\beta|^2 + f_d|\alpha|^2 + f_v \\ \langle S_{hv}S_{hv}^* \rangle &= f_v/3 \\ \langle S_{vv}S_{vv}^* \rangle &= f_s + f_d + f_v \\ \langle S_{hh}S_{vv}^* \rangle &= f_s\beta + f_d\alpha + f_v/3 \\ \langle S_{hh}S_{hv}^* \rangle &= \langle S_{vv}S_{hv}^* \rangle = 0 \end{aligned} \quad (15)$$

where f_s, f_d, and f_v are the surface, double-bounce, and volume scatter contributions, and α and β correspond to the co-polarized correlations of double-bounce and surface scattering, respectively. The contribution of each reflection mechanism to the span P is obtained as [8]

$$P = P_s + P_d + P_v \equiv \left(|S_{hh}|^2 + 2|S_{hv}|^2 + |S_{vv}|^2\right) \quad (16)$$

with

$$\begin{aligned} P_s &= f_s\left(1 + |\beta|^2\right) \\ P_d &= f_d\left(1 + |\alpha|^2\right) \\ P_v &= 8f_v/3. \end{aligned} \quad (17)$$

The decomposition results are depicted in **Figure 2** utilizing the MUSIC optimal vectors of model order four: Backscattering at the forest ground and for some segments close to the canopy top is dominated by double-bounce (red) and surface (blue) reflection. Inside the crown arises volume scattering (green).

4 Conclusion

In this paper, three-dimensional images of forested areas have been generated and investigated by processing polarimetric multibaseline InSAR observations using polarimetric spectral analysis methods. The polarimetric MUSIC algorithm and to a certain extent polarimetric Capon are approriate to extract several backscattering contributions within one azimuth-range resolution cell employing five tracks. LIDAR measurements validate that a phase center at the forest ground is recognized and that the other reflection components are distributed inside the volume. Subsequently, the optimal polarization vectors have been examined by polarimetric decomposition: At the forest ground and near its top, double-bounce and surface reflection is dominant, in the middle of the canopy volume scattering preponderates.

References

[1] S. R. Cloude, K. P. Papathanassiou: *Polarimetric SAR interferometry*, IEEE Trans. Geoscience Remote Sensing, vol. 36, pp. 1551-1565, Sept. 1998.

[2] K. P. Papathanassiou, S. R. Cloude: *Single-Baseline Polarimetric SAR Interferometry*, IEEE Trans. Geoscience Remote Sensing, vol. 39, pp. 2352-2363, Nov. 2001.

[3] S. R. Cloude, K. P. Papathanassiou: *Three stage inversion process for polarimetric SAR interferometry*, IEEE Proc.-Radar Sonar Navig., vol. 150, pp. 125-134, June 2003.

[4] S. R. Cloude: *Dual-baseline coherence tomography*, IEEE Geoscience and Remote Sensing Letters, vol. 4, no. 1, pp. 127-131, Jan. 2007.

[5] A. Reigber, A. Moreira: *First Demonstration of Airborne SAR Tomography Using Multibaseline L-Band Data*, IEEE Trans. Geoscience Remote Sensing, vol. 38, no. 5, pp. 2142-2152, Sept. 2000.

[6] S. Sauer: *Interferometric SAR Remote Sensing of Urban Areas at L-Band Using Multibaseline and Polarimetric Spectral Analysis Techniques*, Ph.D. thesis, University of Rennes 1, Rennes, France, March 2008.

[7] S. Sauer, L. Ferro-Famil, A. Reigber, and E. Pottier: *Polarimetric Dual-baseline InSAR Building Height Estimation at L-Band*, IEEE Geoscience and Remote Sensing Letters, vol. 6, no. 3, pp. 408-412, July 2009.

[8] A. Freeman and S. L. Durden: *A Three-Component Scattering Model for Polarimetric SAR Data*, IEEE Trans. Geoscience and Remote Sensing, vol. 36, no. 3, pp. 963-973, May 1998.

[9] I. Hajnsek, F. Kugler, S.-K. Lee, and K. P. Papathanassiou: *Tropical-Forest-Parameter Estimation by Means of Pol-InSAR: The INDREX-II Campaign*, IEEE Trans. Geoscience and Remote Sensing, vol. 47, no. 2, pp. 481-493, Feb. 2009.

[10] S.-K. Lee, F. Kugler, K. Papathanassiou, I. Hajnsek: *The Impact of Temporal Decorrelation Over Forest Terrain in Polarimetric SAR Interferometry*, Proc. of POLinSAR 2009, Jan. 2009.

[11] F. Lombardini, M. Montanari, F. Gini: *Reflectivity Estimation for Multibaseline Interferometric Radar Imaging of Layover Extended Sources*, IEEE Trans. on Signal Processing, vol. 51, pp. 1508-1519, June 2003.